# Human DNA Polymerase λ Diverged in Evolution from DNA Polymerase β toward Specific $Mn^{++}$ Dependence: a Kinetic and Thermodynamic Study†

Giuseppina Blanca,‡ Igor Shevelev,§ Kristijan Ramadan,§ Giuseppe Villani,|| Silvio Spadari,‡ Ulrich Hübscher,§ and Giovanni Maga*,‡

*Istituto di Genetica Molecolare IGM-CNR, Consiglio Nazionale delle Ricerche, via Abbiategrasso 207, I-27100 Pavia, Italy, Institute of Veterinary Biochemistry and Molecular Biology IVB-MB, University of Zürich, Winterthurerstrasse 190, CH-8057 Zürich, Switzerland, and Institut de Pharmacology et de Biologie Structurale, Centre National de la Recherche Scientifique, 205 Route de Narbonne, 310077 Toulouse, Cedex France*

*Received February 4, 2003; Revised Manuscript Received May 8, 2003*

ABSTRACT: The recently discovered human DNA polymerase λ (DNA pol λ) has been implicated in translesion DNA synthesis across abasic sites. One remarkable feature of this enzyme is its preference for $Mn^{2+}$ over $Mg^{2+}$ as the activating metal ion, but the molecular basis for this preference is not known. Here, we present a kinetic and thermodynamic analysis of the DNA polymerase reaction catalyzed by full length human DNA pol λ, showing that $Mn^{2+}$ favors specifically the catalytic step of nucleotide incorporation. Besides acting as a poor coactivator for catalysis, $Mg^{2+}$ appeared to bind also to an allosteric site, resulting in the inhibition of the synthetic activity of DNA pol λ and in an increased sensitivity to end product (pyrophosphate) inhibition. Comparison with the closely related enzyme human DNA pol β, as well as with other DNA synthesising enzymes (mammalian DNA pol α and DNA pol δ, *Escherichia coli* DNA pol I, and HIV-1 reverse transcriptase) indicated that these features are unique to DNA pol λ. A deletion mutant of DNA pol λ, which contained the highly conserved catalytic core only representing the C-terminal half of the protein, showed biochemical properties comparable to the full length enzyme but clearly different from the close homologue DNA pol β, highlighting the existence of important differences between DNA pol λ and DNA pol β, despite a high degree of sequence similarity.

The survival of a cell depends on its ability to faithfully replicate the genetic information stored in the DNA sequence. However, DNA is constantly subjected to various types of damages, and different DNA repair systems have evolved to repair DNA lesions. Despite these mechanisms, some lesions can escape repair and thus block the progress of a growing replication fork because of the inability of replicative DNA polymerases (DNA pols)[1] to bypass damaged sites (*1*, *2*). Recently, a novel class of enzymes specialized in translesion DNA synthesis has been characterized in eukaryotic cells (*3*). Among them is the recently discovered DNA pol λ. The gene encoding DNA pol λ was cloned and mapped to mouse chromosome 19 and to human chromosome 10 (*4*, *5*). DNA pol λ contains all the critical residues involved in DNA binding, nucleotide binding, nucleotide selection, and catalysis of DNA polymerization and has been assigned to family X based on sequence homology with DNA pol β, DNA pol μ, and terminal deoxynucleotidyltransferase (Tdt). DNA pol λ has been suggested to play a role in meiotic recombination and DNA repair, and the recent demonstration of an intrinsic 5′-deoxyribose-5-phosphate lyase activity in DNA pol λ supports a function of this enzyme in base excision repair (*4*, *5*). Cloned and purified human DNA pol λ inserts nucleotides in a DNA template-dependent manner and is processive in small gaps containing a 5′-phosphate group. These properties, together with its nucleotide insertion fidelity parameters and lack of proofreading activity, indicate that DNA pol λ is a novel DNA pol β-like enzyme (*5*). The incorporation reaction is thermodynamically driven by the establishment of favorable stacking and hydrogen bonding interactions between the template and the incoming nucleotide (*6*). An essential role is played by the twin divalent cations present in the active site, which coordinate the phosphate groups of the incoming nucleotide ensuring proper positioning for the catalytic step (*7*). Eukaryotic DNA pols prefer $Mg^{2+}$ as the activating ion, with two relevant exceptions: DNA pol β and DNA pol λ, which show a strong preference for $Mn^{2+}$. Direct DNA polymerization reaction analysis performed on crystals of the DNA pol β ternary complex in the presence of $Mn^{2+}$ indicated that it promoted greater reactivity than $Mg^{2+}$ at the catalytic site, thereby allowing the nucleotidyl transfer reaction to take place with little or no regard to instructions from a template (*8*). According to these observations, when challenged with $Mn^{2+}$, replicative DNA pols show a decrease in fidelity and an increased ability to tolerate mispaired bases and to replicate

† This work was supported by the CNR Target Project on Biotechnology and CNR Agenzia 2000 (to S.S. and G.M.), by the EU Project No. QLK3-CT-202-02071 REBIOTECH (to G.M. and U.H.), by the Swiss National Science Foundation (Grant 31-61361.00) to K.R., by the Kanton of Zürich to I.S., G.M. (in part), and U.H., and Grant 4373 from the Association pour la Recherche sur le Cancer to G.V.

* Corresponding author. Fax: #39-(0382)422286. E-mail: maga@igm.cnr.it.

‡ Consiglio Nazionale delle Ricerche.

§ University of Zürich.

|| Centre National de la Recherche Scientifique.

[1] Abbreviations: DNA pol, DNA polymerase; dNTPs, 2′-deoxynucleoside triphosphates; dTTP, 2′-deoxythymidine triphosphate; dCTP, 2′-deoxycytidine triphosphate; dGTP, 2′-deoxyguanosine triphosphate; dATP, 2′-deoxyadenosine triphosphate; BRCT-domain, BRCA1 C-terminus-like domain.

10.1021/bi034198m CCC: $25.00 
Published on Web 05/31/2003

across damaged DNA (*9*). Under this respect, DNA pol $\lambda$ represents a remarkable exception. In fact, similarly to DNA pol $\beta$, it has been shown to efficiently bypass an abasic site in the presence of $Mn^{2+}$; however, its fidelity of DNA synthesis was shown to be 5−6-fold higher than DNA pol $\beta$ even under mutagenic conditions (*10*, *11*). Moreover, contrary to replicative DNA pols, DNA pol $\lambda$ did not show significant misincorporation ability in the presence of $Mn^{2+}$ as the metal activator (*11*). Given the mutagenic potential of $Mn^{2+}$ and the proposed role of DNA pol $\lambda$ in translesion synthesis, it was of interest to investigate in detail the effects of $Mg^{2+}$ and $Mn^{2+}$ on the nucleotide incorporation reaction catalyzed by DNA pol $\lambda$, in comparison with other DNA pols.

## MATERIALS AND METHODS

*Chemicals*. [$^3$H]dTTP (40 Ci/mmol) and [$\alpha$-$^{32}$P]dCTP (3000 Ci/mmol) were from Amersham Biosciences; unlabeled dNTPs, DNA poly(dA), oligo(dT)$_{12-18}$, and d24-mer and d66-mer oligodeoxynucleotides were from Roche Molecular Biochemicals. Activated calf thymus DNA was prepared as described (*12*). Whatman was the supplier of the GF/C filters. All other reagents were of analytical grade and were purchased from Merck or Fluka.

*Nucleic Acid Substrates*. The singly primed d24:d66-mer was prepared as follows: the d66-mer template oligonucleotide was mixed with the complementary labeled d24-mer primer oligonucleotide in a 1:1 molar ratio in 20 mM Tris-HCl (pH 8.0) containing 20 mM KCl and 1 mM EDTA, heated at 90 °C for 5 min, and then incubated at 65 °C for 2 h and slowly cooled at room temperature.

The sequence of the d66-mer oligonucleotide was 5′-AGGATGTATGTTTAGTAGGTACATAACTATCTATT-GATACAGACCTAAAACAAAAAATTTTCCGAG3′. The sequence of the d24-mer oligonucleotide was 5′CTCG-GAAAATTTTTTGTTTTAGGT3′.

*Enzymes and Proteins.* Calf thymus DNA pol $\alpha$ and DNA pol $\delta$ were purified as described (*12*), and they had specific activities of 25 000 units/mL (0.2 mg/mL) for DNA pol $\alpha$ and 50 000 units/mL (0.1 mg/mL) for DNA pol $\delta$. One unit of DNA pol activity corresponds to the incorporation of 1 nmol of total dTMP into acid-precipitable material for 60 min at 37 °C in a standard assay containing 0.5 $\mu$g (nucleotides) of DNA poly(dA)/oligo(dT)$_{10:1}$ and 20 $\mu$M dTTP. Recombinant human DNA pol $\lambda$ was expressed and purified as described (*11*). The DNA pol $\lambda\Delta$N mutant (aa 244−575) was generated by PCR. The truncated product was then cloned and expressed as described (*11*). Human DNA pol $\beta$ was from Trevigen. *Escherichia coli* DNA pol I (Klenow fragment) was from Roche Molecular Biochemicals. Recombinant HIV-1 RT was isolated as described (*13*).

*Enzymatic Assays. DNA Polymerase Assay*. DNA pol $\alpha$, $\delta$, $\lambda$, and *E. coli* DNA pol I activities on DNA poly(dA)/oligo(dT)$_{10:1}$ were assayed in a final volume of 25 $\mu$L containing 50 mM Tris-HCl (pH 7.6), 0.25 mg/mL bovine serum albumin, 1 mM DTT, 5 $\mu$M [$^3$H]dTTP (5 Ci/mmol), and $MgCl_2$ or $MnCl_2$, as indicated in the figure legends. DNA pol $\beta$ activity was assayed in the same conditions on activated DNA in the presence of 10 $\mu$M unlabeled dATP, dGTP, dCTP, and 100 mM KCl. All reactions were incubated for 15 min at 37 °C unless otherwise stated.

Scheme 1

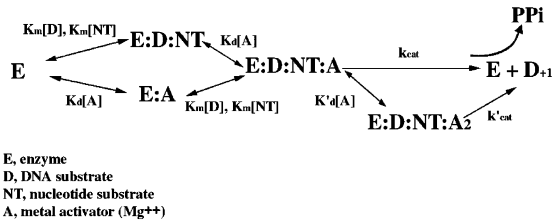


HIV-1 RT activity was assayed as follows: a final volume of 25 $\mu$L contained reaction buffer (50 mM Tris-HCl pH 7.5, 1 mM DTT, 0.2 mg/mL BSA, 4% glycerol), 10 mM $MgCl_2$, 0.5 $\mu$g of DNA poly(rA)/oligo(dT)$_{10:1}$ (0.3 $\mu$M 3′-OH ends), 10 $\mu$M [$^3$H]dTTP (1 Ci/mmol), and 2−4 nM RT. Reactions were incubated at 37 °C for the indicated time. For product analysis, aliquots (20 $\mu$L) were then spotted on glass fiber filters GF/C, which were immediately immersed in 5% ice-cold TCA. Filters were washed twice in 5% ice-cold TCA and once in ethanol for 5 min and dried, and acid-precipitable radioactivity was quantified by scintillation counting.

For incorporation studies with the singly primed d24:d66-mer oligodeoxynucleotide as template, a final volume of 10 $\mu$L contained 50 mM Tris-HCl (pH 7.6), 0.25 mg/mL bovine serum albumin, 1 mM dithiothreitol, 20 nM (3′-OH ends) of d24:d66-mer DNA template, and 3$\mu$M [$\alpha$-$^{32}$P]dCTP (300 Ci/mmol). Enzymes, proteins, $MgCl_2$ or $MnCl_2$, and unlabeled dNTPs were added as indicated in the figure legends. All reactions were incubated for 15 min at 37 °C, samples were mixed with denaturing gel loading buffer (95% v/v formamide, 10 mM EDTA, 0.25 mg/mL bromophenol blue, 0.25 mg/mL xylene cyanol), heated at 95 °C for 5 min, and then subjected to electrophoresis on a 7 M urea, 20% DNA polyacrylamide gel. Quantification of the reaction products on the gel was performed using a Molecular Dynamics PhosphorImager and ImageQuant software.

*Inhibition Assay*. DNA pol activity was assayed as described in a final volume of 25 $\mu$L containing $MgCl_2$ or $MnCl_2$ in the presence of increasing fixed amounts of NaPPi as indicated in the figure legends. All reactions were incubated for 15 min at 37 °C unless otherwise stated, and the DNA was precipitated with 5% trichloroacetic acid. Insoluble radioactive material was determined by scintillation counting as described.

*Kinetic Parameters Calculation.* The dependence of the reaction velocities from $Mg^{2+}$ concentration was analyzed by fitting the data to the equation describing the binding of a mixed activator/inhibitor (*14*):

$$v = \frac{V_{max}}{1 + \frac{K_m}{[S]} + \frac{K_d}{[A]} + \frac{K_m K_d}{[A][S]} + \frac{[A]}{K'_d}} \qquad (1)$$

where $V_m$ is the maximal velocity of the reaction; $K_m$ is the affinity constant for the substrate [S]; and $K_d$ and $K'_d$ represent the equilibrium dissociation constants for the binding of the activator [A] to the first and second binding site, according to the reaction pathway shown in Scheme 1.

The inhibition of the $Mn^{2+}$-dependent nucleotide incorporation reaction by increasing concentration of $Mg^{2+}$ was

analyzed by fitting the experimental data to the equation for a mixed inhibitor (*14*):

$$v = \frac{\dfrac{V_{max}}{\left(1 + \dfrac{[Mg^{++}]}{K'_d}\right)}}{1 + \dfrac{K_m}{[Mn^{++}]}\dfrac{\left(1 + \dfrac{[Mg^{++}]}{K'_d}\right)}{\left(1 + \dfrac{[Mg^{++}]}{K_d}\right)}} \quad (2)$$

where $K_d$ and $K'_d$ are as defined in Scheme 1, and $K_m$ is the apparent affinity constant for $Mn^{2+}$, which is treated here as the variable substrate of the reaction. The end-product inhibition by PPi in dependence of the nucleotide substrate concentrations was fitted to a fully competitive mechanism of inhibition.

*Thermodynamic Parameters Calculation.* $\Delta\Delta G$ values were calculated according to the equation $\Delta\Delta G = RT \ln(K)$, where $K$ is the ratio of the two kinetic constants to be compared, $T$ is the absolute temperature (in K), and $R$ is the gas constant.

$\Delta H$ and $\Delta S$ values were determined according to the Eyring equation

$$\ln(k_{cat}/T) = -\Delta H/T + \ln(k_b/h) + \Delta S/R$$

where $k_b$ is the Boltzmann's constant, $h$ is the Planck's constant, $R$ is the gas constant, and $T$ the absolute temperature (in K).

$\Delta G$ was calculated from the equation

$$\Delta G = \Delta H - T\Delta S$$

## RESULTS

*DNA Polymerase λ Preferentially Utilizes $Mn^{++}$ as the Activating Metal.* Activation of DNA pol λ and its close relative DNA pol β by either $Mg^{2+}$ or $Mn^{2+}$ was tested in a DNA polymerase assay. As shown in Figure 1A, both DNA pol λ and DNA pol β displayed almost 4-fold better activity in the presence of $Mn^{2+}$ than with $Mg^{2+}$. However, DNA pol λ showed the same optimal concentration (2 mM) for both ions, whereas the best $Mg^{2+}$ concentration for DNA pol β was around 5 mM. Since the closely related enzyme Terminal Transferase (Tdt) has been shown to have an unusual preference for $Co^{2+}$ as the activating metal, DNA pol λ and β were tested also in the presence of increasing $Co^{2+}$ concentrations. As shown in Figure 1A, both enzymes were able to utilize $Co^{2+}$ as an activator with similar efficiency to $Mn^{2+}$. This was in agreement with their observed homology with Tdt. DNA pol λ and β were tested also in the presence of different divalent cations, namely, $Zn^{2+}$, $Be^{2+}$, and $Fe^{2+}$. As shown in Figure 1B, both enzymes had similar profiles of activation with the exception of $Zn^{2+}$, which showed optimal stimulation of DNA pol λ at 0.5 mM and of pol β at 2 mM. $Fe^{2+}$ and $Zn^{2+}$, however, were 5−10-fold less efficient than $Mn^{2+}$ as activators of both DNA pols, whereas $Be^{2+}$ was not utilized. In comparison, the replicative DNA pols α and δ had a $Mn^{2+}$ optimum at about 0.1−0.5 mM (Figure 1C, left panel), whereas the optimal activation with $Mg^{2+}$ occurred at 10 mM (Figure 1C, right panel). As

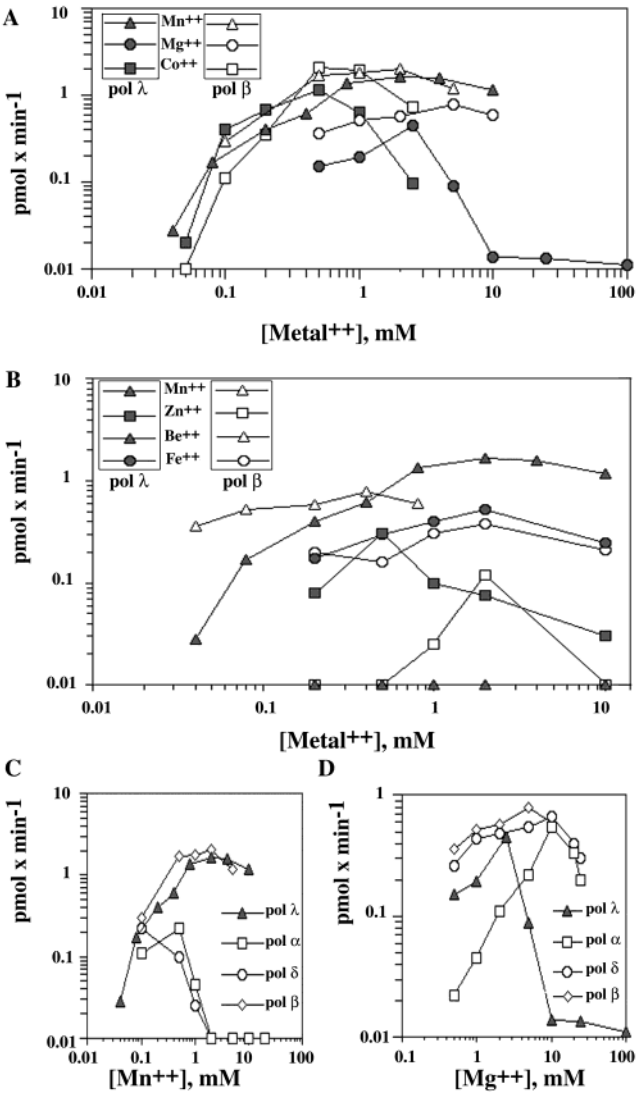


FIGURE 1: Comparative analysis of metal ion activation for various eukaryotic DNA pols. (A) Dependence of DNA pol λ (closed symbols) or DNA pol β (open symbols) activity from $Mn^{2+}$ (triangles), $Mg^{2+}$ (circles), or $Co^{2+}$ (squares). Reactions were carried out as described in the Materials and Methods. (B) Dependence of DNA pol λ (closed symbols) or DNA pol β (open symbols) activity from $Mn^{2+}$, $Zn^{2+}$, $Be^{2+}$, and $Fe^{2+}$. Note the log scale on both axes. (C) Dependence from the $Mn^{2+}$ concentration of the DNA polymerase activity of DNA pol λ (triangles), DNA pol α (squares), DNA pol δ (circles), or DNA pol β (rombics). (D) Dependence from the $Mg^{2+}$ concentration of the DNA polymerase activity of DNA pol λ (triangles), DNA pol α (squares), DNA pol δ (circles), or DNA pol β (rombics). Note the log scale on both axes.

expected, both DNA pol α and DNA pol δ preferred $Mg^{2+}$ as the activating ion. By comparing the activation profiles of the different DNA pols shown in Figure 1, it can be observed that concentrations of $Mn^{2+}$ above 1 mM strongly inhibited both DNA pol α and DNA pol δ, whereas DNA pol λ and β still retained more than 50% of their activity at 10 mM $Mn^{2+}$ (Figure 1A,B). Conversely, DNA pol β, α, and δ showed significant activity at 10−30 mM $Mg^{2+}$ (Figure 1C), whereas DNA pol λ was completely inhibited at 4 mM $Mg^{2+}$. Since the auxiliary factor PCNA has been shown to increase the processivity of pol λ, we tested whether it influenced also the activation by metals. Increasing concentrations of $Mn^{2+}$ or $Mg^{2+}$ were titrated in a DNA pol λ assay in the absence or in the presence of increasing

Table 1: Kinetic Parameters for the Interaction of Full Length DNA Polymerase λ and the N-Terminal Mutant DNA pol λΔN with Their Substrates in the Presence of 1 mM $Mn^{++}$ or $Mg^{++}$

| | DNA polymerase λ | | | | | | DNA polymerase λΔN | | | | | |
|---|---|---|---|---|---|---|---|---|---|---|---|---|
| | $K_m$ | | $k_{cat}$ ($s^{-1}$) | | $k_{cat}/K_m$ ($M^{-1}$ $s^{-1}$) | | $K_m$ | | $k_{cat}$ ($s^{-1}$) | | $k_{cat}/K_m$ ($M^{-1}$ $s^{-1}$) | |
| substr | $Mn^{2+}$ | $Mg^{2+}$ | $Mn^{2+}$ | $Mg^{2+}$ | $Mn^{2+}$ | $Mg^{2+}$ | $Mn^{2+}$ | $Mg^{2+}$ | $Mn^{2+}$ | $Mg^{2+}$ | $Mn^{2+}$ | $Mg^{2+}$ |
| 3′-OH | 75 nM | 43 nM | 0.02 | 0.004 | $2.8 \times 10^5$ | $0.9 \times 10^5$ | 15 nM | 42 nM | 0.018 | 0.007 | $1.2 \times 10^6$ | $0.2 \times 10^6$ |
| TTP | 3.2 μM | 4.7 μM | 0.016 | 0.006 | $5 \times 10^3$ | $1.2 \times 10^3$ | 6.9 μM | 11 μM | 0.016 | 0.005 | $2.2 \times 10^3$ | $0.4 \times 10^3$ |
| PPi | 90 μM[a] | 36 μM[a] | | | | | 42 μM[a] | 8 μM[a] | | | | |
| | −PCNA | +PCNA | | | | | | | | | | |
| $Mg^{2+}$ | 0.4 mM[b] | 0.45 mM[c]<br>0.54 mM[d]<br>0.42 mM[e] | | | | | 0.7 mM[b] | | | | | |
| | −PCNA | +PCNA | | | | | | | | | | |
| $Mn^{2+}$ | 0.3 mM[b] | 0.32 mM[c]<br>0.35 mM[d]<br>0.33 mM[e] | | | | | 0.15 mM[b] | | | | | |

[a] $K_i$ value derived from inhibition studies. [b] $K_d$ value for activation. [c−e] $K_d$ values for activation by $Mn^{2+}$ or $Mg^{2+}$ in the presence of 50, 15, and 300 ng of PCNA, respectively.

amounts of PCNA. As reported in Table 1, the calculated $K_d$ for $Mn^{2+}$- or $Mg^{2+}$-dependent activation did not change significantly upon addition of PCNA.

*$Mg^{++}$ Is Both an Activator and an Inhibitor of DNA Polymerase λ.* The catalytic efficiency DNA pol λ was investigated in dependence of increasing concentrations of either $Mn^{2+}$ or $Mg^{2+}$. All the calculated kinetic constants are summarized in Table 1. Initial velocities of the reaction were measured in the presence of increasing concentrations of substrate (either nucleotide or DNA). Measurements for each set of variable substrate concentrations were done in the presence of different metal ion concentrations (either $Mg^{2+}$ or $Mn^{2+}$). From each curve, the kinetic parameters $K_m$ and $k_{cat}$ for the analyzed substrate were derived, and their ratio ($k_{cat}/K_m$) representing the efficiency of substrate utilization was calculated. As shown in Figure 2A, in the presence of $Mn^{2+}$ the catalytic efficiency $k_{cat}/K_m$ for nucleotide incorporation was increased. When similar experiments were repeated with $Mg^{2+}$, both activation and inhibition occurred since the catalytic efficiency for nucleotide incorporation was increased at $Mg^{2+}$ below 2 mM but was strongly reduced at higher concentrations (Figure 2C). Similar results were obtained when the reaction velocities were measured over a range of different concentrations of the DNA substrate, with $Mn^{2+}$ acting as a pure activator (Figure 2B) and $Mg^{2+}$ as a mixed activator/inhibitor (Figure 2D).

*$Mg^{++}$ Binds to DNA Polymerase λ with Different Affinities as an Activator or an Inhibitor.* The reaction velocities measured at different concentrations of the substrates (either nucleotide or DNA) were plotted in dependence of either $Mn^{2+}$ or $Mg^{2+}$ concentrations. In the case of $Mn^{2+}$, the dependence from the metal activator fitted to a hyperbolic relationship with both substrates (Figure 3A,C), from which an apparent dissociation constant ($K_d$) of 0.5 mM for the metal was estimated. On the contrary, dependence of the reaction velocities from $Mg^{2+}$ followed a more complex pattern, consistent with a mixed activation/inhibition mechanism (Figure 3B,D). A possible reaction mechanism is summarized in Scheme 1 and is described by eq 1 (see Materials and Methods). According to this model, $Mg^{2+}$ can bind to the [E:D:NT] complex with a dissociation constant $K_d$. This complex will then give products with a breakdown rate $k_{cat}$. In addition, $Mg^{2+}$ can bind to the [E:D:NT:A] complex with a dissociation constant $K'_d$, which will then give products with a rate $k'_{cat}$. Whether such a mechanism gives rise to activation or inhibition depends on the relative values of all the four constants. Assuming that $k'_{cat} < k_{cat}$, if $K_d$ is very large, then the metal will act as an inhibitor, if conversely, $K'_d$ is very large, then the metal will behave as an activator. In the intermediate cases, both constants will make a contribution giving a mixed activation/inhibition pattern, as was observed here. Fitting the curves to eq 1 yielded two $K_d$ values for $Mg^{2+}$: one of 0.5−0.6 mM, very close to the $K_d$ measured for $Mn^{2+}$ and corresponding to the activating part of the curve, and a second $K_d$ value of 2.2−

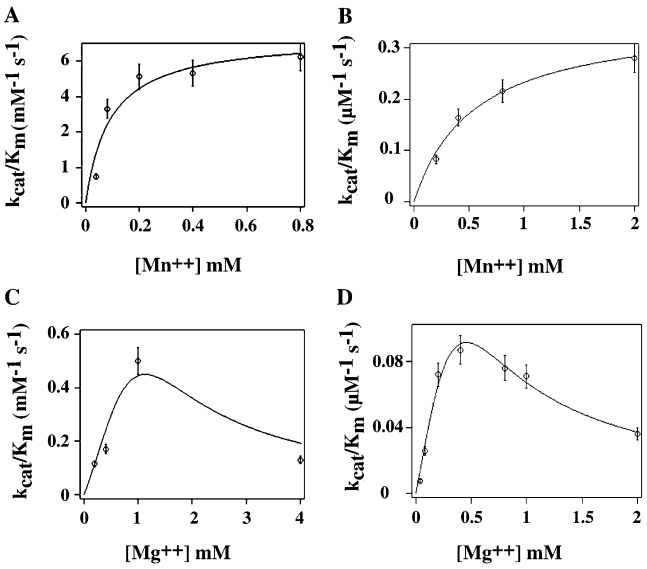


FIGURE 2: Effects of $Mg^{++}$ or $Mn^{++}$ on the substrate utilization by DNA pol λ. Reactions were carried out as described in the Materials and Methods. Data sets shown in panels A and B were fitted to the hyperbolic relationship: $(k_{cat}/K_m)_{obs} = (k_{cat}/K_m)_{max}/(1 + K_d/[A])$, whereas data sets shown in panels C and D were fitted to eq 1 (see Materials and Methods) where $v$ was replaced by $(k_{cat}/K_m)_{obs}$ and $V_{max}$ by $(k_{cat}/K_m)_{max}$. (A) Dependence from the $Mn^{2+}$ concentration of the efficiency of nucleotide substrate utilization ($k_{cat}/K_m$ values) for DNA pol λ. (B) Dependence from the $Mn^{2+}$ concentration of the efficiency of DNA substrate utilization ($k_{cat}/K_m$ values) for DNA pol λ. (C) Dependence from the $Mg^{2+}$ concentration of the efficiency of nucleotide substrate utilization ($k_{cat}/K_m$ values) for DNA pol λ. (D) Dependence from the $Mn^{2+}$ concentration of the efficiency of DNA substrate utilization ($k_{cat}/K_m$ values) for DNA pol λ.

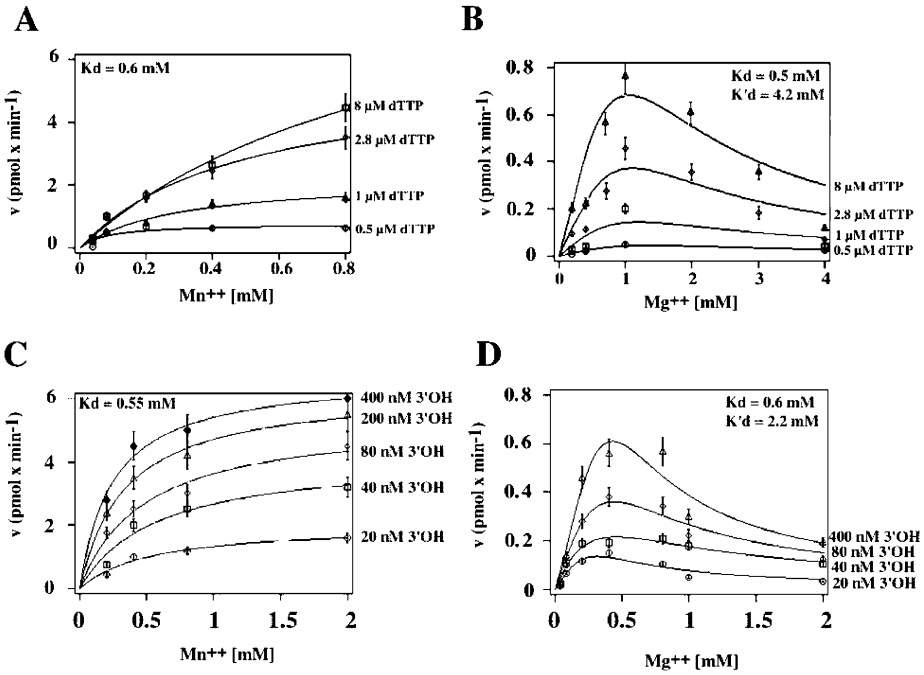


FIGURE 3: Effects of $Mg^{++}$ and $Mn^{++}$ on the reaction velocity of DNA pol λ in dependence of different substrate concentrations. Reactions were carried out as described in the Materials and Methods. Data sets shown in panels A and C were fitted to the hyperbolic relationship $v = V_{max}/(1 + K_d/[Mn^{2+}])$, and data sets shown in panels B and D where fitted to eq 1 (see Materials and Methods). (A) Variation of the reaction velocity of DNA pol λ in dependence of increasing $Mn^{2+}$ (0.05, 0.1, 0.2, 0.4, and 0.8 mM) in the presence of different nucleotide substrate concentrations. Nucleotide (dTTP) concentrations used were 0.5, 1, 2.8, and 8 μM. (B) Variation of the reaction velocity of DNA pol λ in dependence of increasing $Mg^{2+}$ (0.02, 0.04, 0.06, 1, 2, 3, and 4 mM) in the presence of different nucleotide substrate concentrations. Nucleotide (dTTP) concentrations used were 0.5, 1, 2.8, and 8 μM. (C) Variation of the reaction velocity of DNA pol λ in dependence of increasing $Mn^{2+}$ (0.2, 0.4, 0.8, and 2 mM) with different DNA substrate (expressed as available 3′-OH primer ends) concentrations. DNA concentrations used were 20, 40, 80, 200, and 400 nM. (D) Variation of the reaction velocity of DNA pol λ in dependence of increasing $Mg^{2+}$ (0.01, 0.02, 0.03, 0.08, 1, and 2 mM) with different DNA substrate (expressed as available 3′-OH primer ends) concentrations. DNA concentrations used were 20, 40, 80, and 400 nM.

4.2 mM, corresponding to the inhibitory part. These results suggested that $Mg^{2+}$ binds to the active site of DNA pol λ like $Mn^{2+}$ as an activator ($K_d$ = 0.5 mM) but also at a different site with lower affinity ($K'_d$ = 2.2−4.2 mM) as an inhibitor.

*DNA Polymerase λ Has Two Binding Sites for $Mg^{++}$.* To determine the binding mode of $Mg^{2+}$ to DNA pol λ, inhibition of the DNA polymerization reaction by increasing amounts of $Mg^{2+}$ was measured in dependence of varying concentrations of $Mn^{2+}$ as the activator. As shown in Figure 4A, double-reciprocal plots of the data indicated a mixed-type of inhibition. As shown in Figure 4B, $Mg^{2+}$ decreased both the apparent $K_d$ for $Mn^{2+}$ and the $k_{cat}$ of the reaction. A mixed-inhibition system where, according to the proposed mechanism of the reaction (Scheme 1), $Mg^{2+}$ binds to the active site with the $K_d$ binding costant and to the allosteric with the $K'_d$ affinity constant is described by eq 2. The values of both constants can be derived from secondary plots of the intercepts and the slopes of the curves shown in Figure 4A, against the $Mg^{2+}$ concentrations. As shown in Figure 4C, a replot of the slopes versus $Mg^{2+}$ concentrations revealed a $K_d$ value of 0.4 mM, whereas a replot of the intercepts (shown as an inset of Figure 4C), yielded a $K'_d$ value of 2.5 mM. To confirm the inhibition mechanism, a broader range of $Mg^{2+}$ concentrations were tested in the presence of different $Mn^{2+}$ concentrations as the activator. Figure 4C shows the variation of the initial velocities of the reaction in dependence of the $Mg^{2+}$ concentrations. Analysis of the data by the method of Dixon again revealed a mixed-inhibition pattern with the lines intersecting below the *x*-axis (Figure 4C, inset). From this plot, a $K'_d$ value of 2.8 mM was calculated. These findings indicated that the competition between $Mg^{2+}$ and $Mn^{2+}$ cannot be described by a simple linear model (either competitive or noncompetitive). The values of the $K_d$ and $K'_d$ constants derived form these inhibition studies were perfectly comparable with those calculated from the activation studies shown in Figure 3, further reinforcing the notion that $Mg^{2+}$ can bind to two distinct sites of DNA pol λ.

*$Mg^{++}$ Increases the Distributivity of DNA Polymerase λ.* The effect of increasing concentrations of $Mg^{2+}$ on the DNA synthesis catalyzed by DNA pol λ on the heteropolymeric DNA template d24:d66-mer in the presence of 1 mM $Mn^{2+}$ was analyzed by denaturing gel electrophoresis and autoradiography of the synthesized products. As shown in Figure 5A, lane 1, in the absence of $Mg^{2+}$ most of the synthesized products were between 30 and 50 nt in size, as the result of strong termination at several pausing sites along the template, with only a small amount of full length 66 nt products. Quantification of the synthesized products revealed that addition of $Mg^{2+}$ showed different effects depending on its concentration. Between 1 and 5 mM, $Mg^{2+}$ mostly abolished the ability of DNA pol λ to overcome the first pausing site, causing the disappearance of the products longer than 30−35 nt (compare lanes 2−4 with lane 1), whereas at higher concentrations it completely suppressed DNA synthesis (lanes 5−7). Thus, the observed increase in distributivity of DNA pol λ was interpreted as a result of the lower nucleotide incorporation efficiency when $Mg^{2+}$ is the activating ion (Table 1). At higher concentrations, $Mg^{2+}$ behaved as an

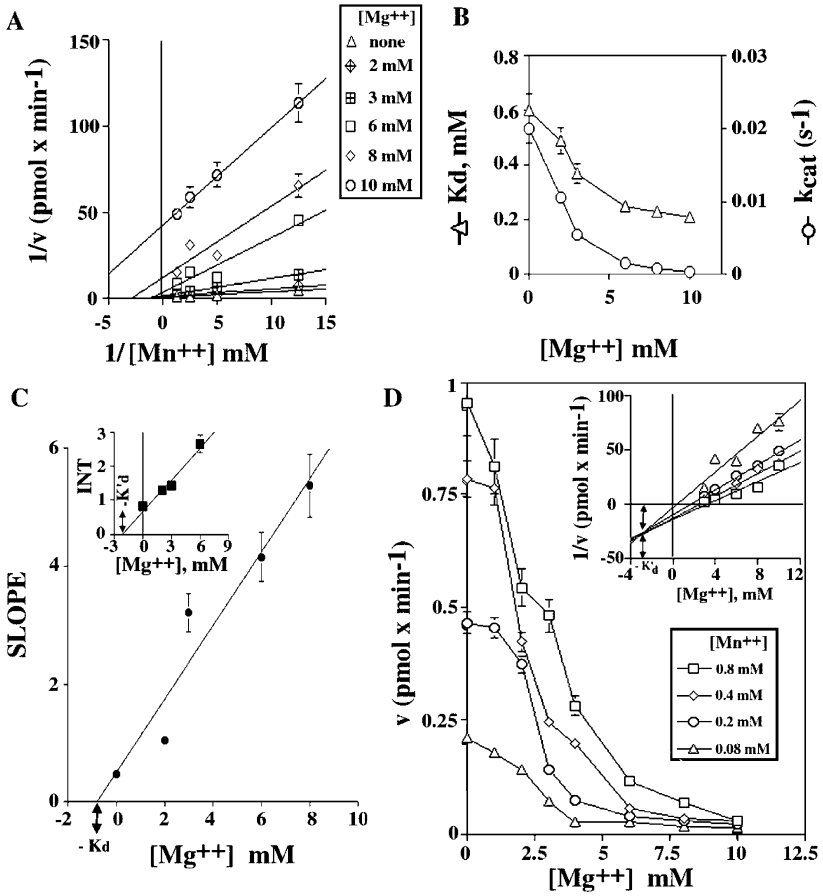


FIGURE 4: Inhibition by $Mg^{++}$ of the $Mn^{++}$-dependent DNA DNA polymerase activity of DNA pol $\lambda$. Reactions were carried out as described in the Materials and Methods. (A) Effects of increasing $Mg^{2+}$ concentrations on the $Mn^{2+}$-dependent DNA polymerase activity of DNA pol $\lambda$. $Mn^{2+}$ concentrations tested were 0.04, 0.2, 0.4, and 0.8 mM. Data were analyzed by the double-reciprocal (Lineweaver−Burk) plot. (B) Variation of the apparent affinity for $Mn^{2+}$ ($K_d$) and of the reaction rate ($k_{cat}$) of DNA pol $\lambda$ in dependence of the $Mg^{2+}$ concentration. $K_d$ and $k_{cat}$ values at each $Mg^{2+}$ concentration were calculated from the experiments shown in panel A according to eq 2 (see Materials and Methods). (C) Secondary plot of the variation of the slopes of the curves shown in panel A in dependence of the $Mg^{2+}$ concentrations. Inset: secondary plot of the variation of the *y* axis intercepts (INT) of the curves shown in panel A in dependence of the $Mg^{2+}$ concentrations. (D) Variation of the initial velocity values of the reaction catalyzed by DNA pol $\lambda$ measured at different $Mn^{2+}$ concentrations (0.08, 0.2, 0.4, and 0.8 mM) in dependence of increasing $Mg^{2+}$ (1, 2, 3, 4, 6, 8, and 10 mM). Inset: Dixon plot of the data, showing a mixed-type inhibition mechanism.

inhibitor, abolishing the activity of DNA pol $\lambda$. To verify whether the decrease in processivity was an intrinsinc property of $Mg^{2+}$ when acting as the metal activator of DNA pol $\lambda$, DNA synthesis was measured in the presence of either 1 mM $Mn^{2+}$ or 1 mM $Mg^{2+}$ on the d24:d66-mer template, under limited incorporation conditions. As shown in Figure 5B, addition of the first encoded nucleotide only resulted in similar accumulation of the expected +1 product (compare lane 3 with lane 6). However, when synthesis was allowed to proceed up to positions +2 and +4, by addition of the appropriate nucleotide combinations, DNA pol $\lambda$ showed higher distributivity in the presence of $Mg^{2+}$ than with $Mn^{2+}$ (compare lane 2 with lane 5 and lane 1 with lane 4), as revealed by the accumulation of intermediate products. Together, these results indicated that $Mg^{2+}$ as an activator increased the distributivity of DNA pol $\lambda$.

*DNA Polymerase λ Shows an Unusual Sensitivity to Pyrophosphate Inhibition.* According to the reaction pathway in Scheme 1 (see Materials and Methods), the end products of the DNA polymerization reaction are an elongated DNA polynucleotide chain and inorganic PPi. Usually, the large equilibrium dissociation constant for PPi renders the DNA polymerization reaction practically irreversible under physiological conditions. Recently, it has been found that HIV-1 RT has a low equilibrium constant for PPi binding and effectively reverses the DNA polymerization reaction through pyrophosphorolytic removal of the last incorporated nucleotide. End-product inhibition studies were performed with DNA pol $\lambda$, DNA pol α, DNA pol $\beta$, HIV-1 RT, and *E. coli* DNA pol I (Kleenow fragment) in the presence of $Mg^{2+}$ as the activating ion, and the inhibition profiles are shown in Figure 5C, left panel. As expected, HIV-1 RT was the most sensitive to PPi inhibition, whereas DNA pol $\beta$, DNA pol α, and *E. coli* DNA pol I were much less inhibited. Unexpectedly, DNA pol $\lambda$ showed a sensitivity to PPi inhibition very close to the one of HIV-1 RT. When the inhibition by PPi was measured in the presence of $Mn^{2+}$ as the activating ion, DNA pol $\lambda$ was less sensitive to PPi inhibition than with $Mg^{2+}$ (Figure 5C, right panel), whereas DNA pol $\beta$ showed an opposite behavior, with a much higher sensitivity to PPi inhibition in the presence of $Mn^{2+}$ than $Mg^{2+}$. The mechanism of inhibition was found to be competitive with the nucleotide substrate for all the enzyme tested (as shown for pol $\lambda$ in Figure 5D). The derived equilibrium dissociation constants ($K_i$) of PPi for DNA pol $\lambda$ are reported in Table 1.

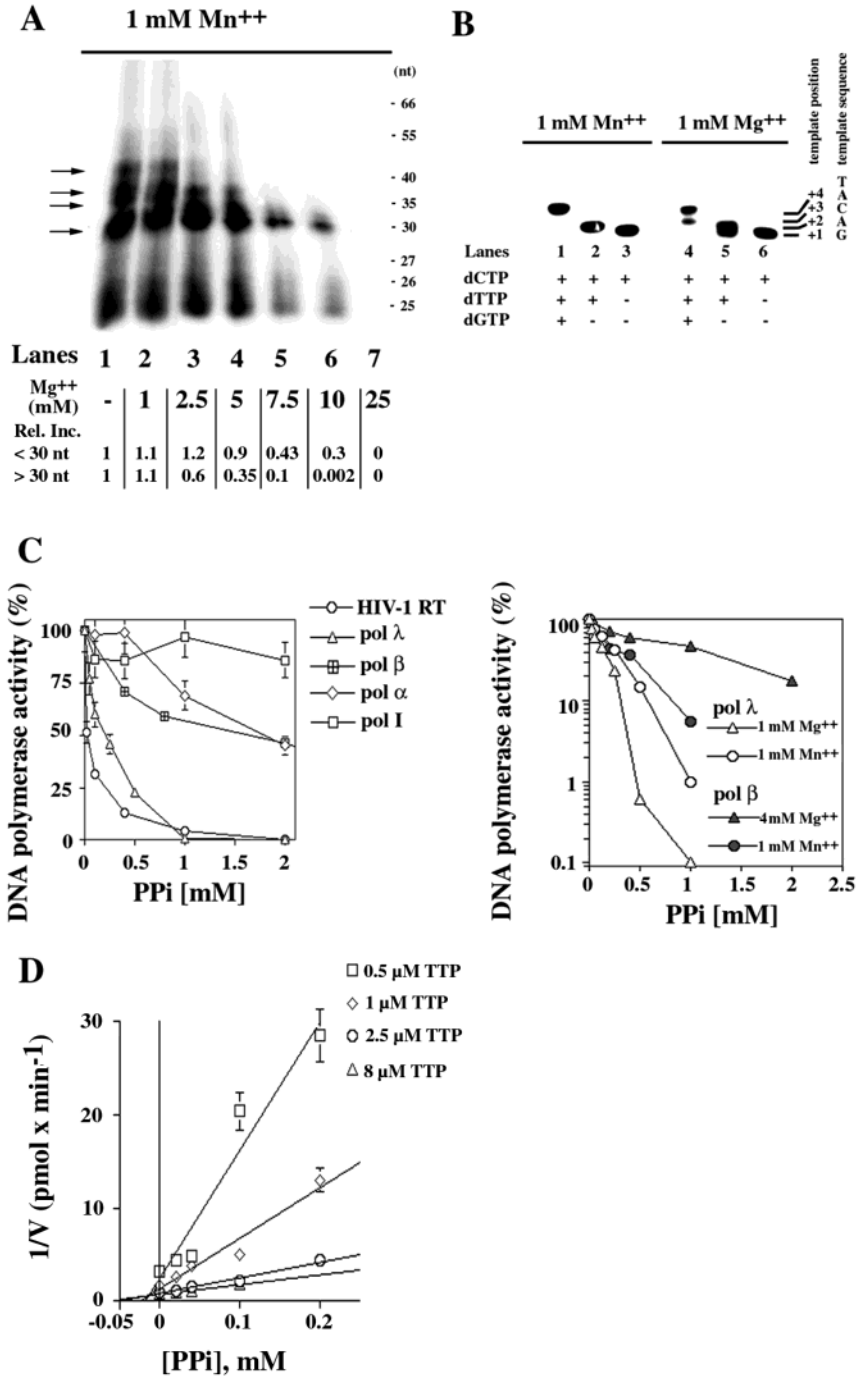


FIGURE 5: $Mg^{++}$ decreases the nucleotide incorporation rate and increases the sensitivity to PPi inhibition of DNA pol λ. Reactions were carried out as described in the Materials and Methods. (A) Effects of increasing $Mg^{2+}$ concentrations on the products of the nucleotide incorporation reaction catalyzed by DNA pol λ with the d24:d66-mer primer/template oligonucleotide substrate in the presence of [α-$^{32}$P] dCTP and unlabeled dATP, dGTP, and dTTP (see Materials and Methods). Size markers (in nucleotides) are shown on the right side of the panel. Arrows indicate the sites of DNA synthesis termination. Products were quantified, normalized to the total intensity of each lane, and expressed as relative values with respect to the reaction in the absence of $Mg^{2+}$ (lane 1). Two quantifications were performed independently for products with size >30 nt (corresponding to the first strong pausing site) and <30 nt. Relative values are indicated at the bottom of each lane. (B) Comparison of $Mg^{2+}$- or $Mn^{2+}$-dependent DNA synthesis catalyzed by DNA pol λ with the d24:d66-mer primer/template oligonucleotide substrate, under limited nucleotide incorporation conditions in the presence of [α-$^{32}$P] dCTP alone (lanes 3 and 6) or in combination with unlabeled dTTP (lanes 2 and 5) or dTTP plus dGTP (lanes 1 and 4). The first four positions of the template sequence are indicated on the right side of the panel. (C) Left panel: inhibition by PPi of the nucleotide incorporation reaction catalyzed by HIV-1 RT (circles), DNA pol λ (triangles), DNA pol β (crossed squares), DNA pol α (rombics), and *E. coli* DNA pol I (squares); right panel: effects of $Mg^{2+}$ (triangles) or $Mn^{2+}$ (circles) on the inhibition by PPi of the nucleotide incorporation reaction catalyzed by DNA pol λ (open symbols) or DNA pol β (closed symbols). (D) Dixon plot of the variation of the initial velocities of the reaction catalyzed by DNA pol λ measured at increasing dTTP concentrations (0.5, 1, 2.5, and 8 μM), in dependence of different PPi concentrations (0.02, 0.04, 0.1, and 0.2 mM). The lines intersect above the *x* axis, indicating a competitive mechanism of inhibition.

*Effect of $Mg^{++}$ and $Mn^{++}$ on the Thermodynamics of the Forward (DNA Polymerization) Reaction Catalyzed by DNA Polymerase λ.* The kinetic constants listed in Table 1 were used to estimate the relative free energy change (ΔΔ*G*) in

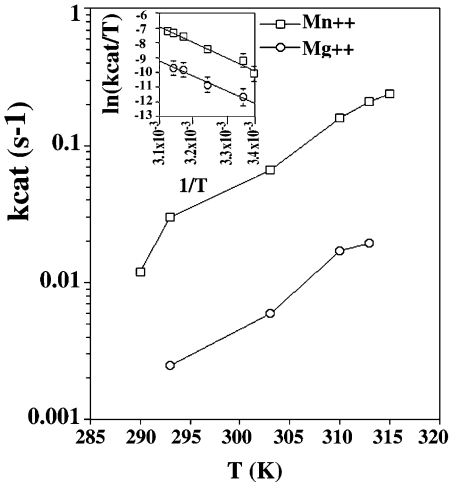


FIGURE 6: Thermodynamic analysis of the $Mn^{++}$- or $Mg^{++}$-dependent activation of the DNA polymerase activity of DNA pol $\lambda$. Variation of the $k_{cat}$ values for nucleotide incorporation of DNA pol $\lambda$ in dependence of the absolute temperature (in K) of the reaction, in the presence of 1 mM $Mn^{2+}$ (squares) or 1 mM $Mg^{2+}$ (circles). Inset: Eyring plot of the data (see Materials and Methods). The $k_{cat}$ values were calculated by fitting the variation of the initial velocities of the reaction in dependence of increasing dTTP concentrations (0.5, 1, 2, 4, 6, and 10 $\mu$M) to the Michaelis−Menten equation $\upsilon = V_{max}/(1 + K_m/[S])$, where [S] is dTTP, $V_{max} = k_{cat}[E]_0$, and $[E]_0$ is the input enzyme concentration. The $\Delta G$ values were calculated from the data as described in the Materials and Methods.

the forward DNA polymerization reaction associated with the replacement of $Mn^{2+}$ with $Mg^{2+}$. Direct comparison of the $k_{cat}$ values obtained in dependence of both DNA and dNTP substrates showed that catalysis was clearly favored in the presence of $Mn^{2+}$, with a $\Delta\Delta G$ between 0.7 and 0.9 kcal $mol^{-1}$. To better understand the molecular basis for the preference of $Mn^{2+}$ over $Mg^{2+}$ by DNA pol $\lambda$, the $k_{cat}$ values for the nucleotide incorporation reaction were measured as a function of the reaction temperature (Figure 6). From the observed variations, it was possible to estimate the $\Delta G$ for the overall reaction (see Materials and Methods). As summarized in Figure 6, the forward reaction was favored in the presence of $Mn^{2+}$ with respect to $Mg^{2+}$ ($\Delta G$ values were of $-$ 0.8 kcal $mol^{-1}$ and $-$ 0.39 kcal $mol^{-1}$ in the presence of $Mn^{2+}$ or $Mg^{2+}$, respectively) with an overall difference of about 0.4 kcal $mol^{-1}$. Thus, $Mn^{2+}$ as the activating metal renders the catalytic step thermodynamically favored.

*Metal Ion Preference and Sensitivity to Pyrophosphate Inhibition Is an Intrinsic Property of the Catalytic Core Domain of DNA Polymerase* $\lambda$. The closest homologue of DNA pol $\lambda$ in eukaryotic cells is the repair enzyme DNA pol $\beta$. On the basis of sequence similarity, both enzymes have been grouped into the family X of nucleotidyltransferases. However, the strong homology between the two proteins is confined to the catalytic domain, which represents the C-terminal half of DNA pol $\lambda$ (aa 244−575). The N-terminal portion of the protein contains a BRCT-like domain (aa 1−132) and a Proline-rich domain (aa 132−244) that are not present in DNA pol $\beta$. The unique behavior showed by DNA pol $\lambda$ with respect to its metal ion preference and sensitivity to end-product inhibition in comparison with the closely related DNA pol $\beta$ might suggest a specific contribution of the N-terminal part of DNA pol $\lambda$. To verify this hypothesis, a truncated form of DNA pol $\lambda$ (named DNA pol$\lambda\Delta$N) comprising the DNA polymerase domain but lacking both the BRCT-like and the Proline-rich domains has been produced and purified. The results of the complete kinetic characterization of DNA pol$\lambda\Delta$N are summarized in Table 1. The enzymatic properties of the truncated enzyme were very similar to the one of the full length protein. Remarkably, the affinity of DNA pol $\lambda$ for the DNA substrate in the presence of $Mn^{2+}$ was enhanced by deletion of the N-terminal part of the protein. As a result, DNA pol$\lambda\Delta$N showed a 10-fold higher efficiency ($k_{cat}/K_m$ value) in DNA substrate binding than the full length protein. Nucleotide binding was favored by $Mn^{2+}$, with respect to $Mg^{2+}$, similarly to the full length protein. The equilibrium dissociation constants for $Mg^{2+}$ and $Mn^{2+}$ were not significantly different between the two enzymes; however, the sensitivity to PPi inhibition with respect to the full length protein was 2-fold higher for the truncated enzyme in the presence of $Mn^{2+}$ and almost 5-fold higher in the presence of $Mg^{2+}$, with equilibrium dissociation constants for PPi binding of 42 and 8 $\mu$M, respectively. These results clearly indicated that the sensitivity to PPi inhibition was not due to the N-terminal domain, which rather played a down-regulation role, but was an intrinsic property of the catalytic core domain of DNA pol $\lambda$, suggesting a different architecture of the active sites of DNA pol $\lambda$ and $\beta$, despite their high sequence identity.

## DISCUSSION

The kinetic analysis presented here indicated that the observed preference of DNA pol $\lambda$ for $Mn^{2+}$ as an activator was due to a higher nucleotide incorporation efficiency with respect to $Mg^{2+}$ (Table 1). These results, together with the observation of a more favorable thermodynamic profile for the nucleotide incorporation reaction catalyzed by DNA pol $\lambda$ in the presence of $Mn^{2+}$ over $Mg^{2+}$, (Figure 6) seem to indicate that DNA pol $\lambda$ evolved as a $Mn^{2+}$-specific enzyme. This might be related to its ability to bypass an abasic site. In fact, detailed kinetic analysis of the abasic site bypass reaction catalyzed by T4 DNA pol showed that substitution of $Mn^{2+}$ for $Mg^{2+}$ significantly enhanced the rate of the conformational change preceding chemistry without a substantial effect on the intrinsic ground-state binding of dNTP opposite an abasic site (*15*). Thus, apparently $Mn^{2+}$ is the optimal ion to stabilize unconventional intrahelical conformations of the incoming dNTPs, such as the ones occurring in front of damaged templates. In light of these observations, DNA pol $\lambda$ apparently optimized its interaction with $Mn^{2+}$ (and thus its ability to bypass an abasic site) by reducing the mutagenic effects usually associated with this cation.

The high homology of DNA pol $\lambda$ with DNA pol $\beta$ is confined to the C-terminal half of the protein (aa 244−575) containing the catalytic site, whereas the N-terminal part bears a BRCT and a Pro-rich domain, which are specific to DNA pol $\lambda$ (*16*). The comparison between intact DNA pol $\lambda$ and a N-terminal deletion mutant presented here showed that the preference for $Mn^{2+}$ over $Mg^{2+}$ was intrinsic to the catalytic core domain of DNA pol $\lambda$, which displayed kinetic properties comparable to the full length enzyme (Table 1). Remarkably, the affinity for DNA of the N-terminal deletion mutant was higher than the full length protein, and DNA binding was more favorable in the presence of $Mn^{2+}$ than with $Mg^{2+}$. Thus, the extra domains present at the N-terminus

of DNA pol λ with respect to DNA pol β appear to play no role in the specificity for $Mn^{2+}$ activation, but rather they seem to be even decreasing the enzyme efficiency.

Another interesting feature of DNA pol λ revealed in this study was its sensitivity to end-product (PPi) inhibition. Inorganic pyrophosphate (PPi) is released from the enzyme upon phosphodiester bond formation and nucleotide incorporation. Albeit condensation of PPi with the last incorporated nucleotide to give a free nucleoside triphosphate and a −1 DNA chain (pyrophosphorolysis, the reverse of the DNA polymerization reaction) is theoretically possible, the large equilibrium dissociation constant of free PPi for the enzyme renders the DNA polymerization reaction practically not reversible. The only known exceptions are viral DNA pols, such as HIV-1 RT and HBV DNA pol, whose ability to phosphorolytically remove the last incorporated nucleotide plays an important role in antiviral drug resistance (*17*−*19*). We compared the sensitivity of DNA pol λ, DNA pol β, DNA pol α, *E. coli* DNA pol I, and HIV-1 RT to PPi inhibition, and we found that, in the presence of $Mg^{2+}$, DNA pol λ was almost 10-fold more inhibited than DNA pol β, with an inhibition profile close to the one of HIV-1 RT (Figure 5C). When $Mn^{2+}$ was the metal activator, however, DNA pol λ was more resistant to PPi inhibition, whereas the sensitivity of DNA pol β was increased. Interestingly, the other pol X family member Tdt has been reported to have a low sensitivity to PPi inhibition, with a $K_i$ of 230 μM, thus again confirming the peculiarity of DNA pol λ with respect to its homologues (*20*).

Our thermodynamic analysis suggested that the apparent catalytic rate ($k_{cat}$) for DNA pol λ was reduced by $Mg^{2+}$. Accordingly, incorporation product analysis showed that $Mg^{2+}$ slowed the rate of nucleotide incorporation, resulting in a more distributive synthesis (Figure 5A,B). The occupancy of the active site by PPi after catalysis, because of its predicted slow dissociation, might explain the reduced rate of nucleotide incorporation by DNA pol λ observed in the presence of $Mg^{2+}$.

Detailed kinetic analysis clearly showed that $Mg^{2+}$ behaved as a mixed activator−inhibitor (Figure 3), with two distinct dissociation constants: one of about 0.5 mM for the activating part and one of about 2.5−5 mM for the inhibiting part. These two $K_d$ values reflected the existence of two distinct binding sites (or two families of binding sites with the same affinity). Binding of $Mg^{2+}$ to the activating site was not mutually exclusive with binding to the inhibiting site (Figure 4). Additional binding sites for metal ions have been already described for Tdt, the endonuclease Fen 1, and DNA pol α. Moreover, crystallization studies of DNA pol β revealed at least three kinds of nonequivalent metal ion binding sites: one catalytic (involving a pair of ions and contributing to stabilize the transition state and to properly position the nucleotide for catalysis) and two involved in DNA binding (*8*, *21*−*23*).

Together, our results indicated that, despite a strong sequence homology, the catalytic cores of DNA pol λ and β might have a different architecture, as reflected by their different biochemical properties. In addition, $Mg^{2+}$ was shown to be a negative regulator of DNA pol λ activity at those concentrations (above 10 mM) that represent the optimal activation range for DNA pol α and δ (Figure 1). It is tempting to speculate that in the presence of low $Mg^{2+}$ and/or high $Mn^{2+}$, which is under unfavorable or even potentially mutagenic conditions for replicative DNA pols, DNA pol λ can nevertheless synthesize DNA with high efficiency and fidelity. The metal ion $Mn^{2+}$ is considered a potential mutagen, particularly based on its effects on the activity of DNA pols. Although the concentrations used in the present study (0.5−1 mM) cannot be considered physiological in absolute terms, it should be noted that free metal ion concentrations are tightly regulated in vivo by special metal ion binding proteins, and their concentrations may vary considerably, even within the nucleus of a cell (*24*). Moreover, in our study we show that DNA pol λ is nevertheless capable of carrying on its functions also in the presence of physiological concentrations of $Mg^{2+}$, albeit with lower efficiency.

## ACKNOWLEDGMENT

We thank Dr. Luis Blanco, Centro de Biologia Molecular Severo Ochoa (CSIC-UAM), Universidad Autonoma, Cantoblanco, Madrid, Spain, for providing us with the plasmid for the expression of recombinant human DNA pol λ.

## REFERENCES

1. Friedberg, E. C., Feaver, W. J., and Gerlach, V. L. (2000) *Proc. Natl. Acad. Sci. U.S.A. 97*, 5681−3.
2. Goodman, M. F. (2002) *Annu. Rev. Biochem. 71*, 17−50.
3. Hübscher, U., Maga, G., and Spadari, S. (2002) *Annu. Rev. Biochem. 71*, 133−63.
4. Garcia-Diaz, M., Dominguez, O., Lopez-Fernandez, L. A., de Lera, L. T., Saniger, M. L., Ruiz, J. F., Parraga, M., Garcia-Ortiz, M. J., Kirchhoff, T., del Mazo, J., Bernad, A., and Blanco, L. (2000) *J. Mol. Biol. 301*, 851−67.
5. Garcia-Diaz, M., Bebenek, K., Sabariegos, R., Dominguez, O., Rodriguez, J., Kirchhoff, T., Garcia-Palomero, E., Picher, A. J., Juarez, R., Ruiz, J. F., Kunkel, T. A., and Blanco, L. (2002) *J. Biol. Chem. 277*, 13184−91.
6. Brautigam, C. A., and Steitz, T. A. (1998) *Curr. Opin. Struct. Biol. 8*, 54−63.
7. Steitz, T. A. (1999) *J. Biol. Chem. 274*, 17395−8.
8. Pelletier, H., Sawaya, M. R., Wolfle, W., Wilson, S. H., and Kraut, J. (1996) *Biochemistry 35*, 12762−77.
9. Villani, G., Tanguy Le Gac, N., Wasungu, L., Burnouf, D., Fuchs, R. P., and Boehmer, P. E. (2002) *Nucleic Acids Res. 30*, 3323−32.
10. Ramadan, K., Shevelev, I. V., Maga, G., and Hubscher, U. (2002) *J. Biol. Chem. 277*, 18454−8.
11. Maga, G., Villani, G., Ramadan, K., Shevelev, I., Le Gac, N. T., Blanco, L., Blanca, G., Spadari, S., and Hubscher, U. (2002) *J. Biol. Chem. 277*, 48434−40.
12. Weiser, T., Gassmann, M., Thommes, P., Ferrari, E., Hafkemeyer, P., and Hubscher, U. (1991) *J. Biol. Chem. 266*, 10420−8.
13. Maga, G., Ramunno, A., Nacci, V., Locatelli, G. A., Spadari, S., Fiorini, I., Baldanti, F., Paolucci, S., Zavattoni, M., Bergamini, A., Galletti, B., Muck, S., Hubscher, U., Giorgi, G., Guiso, G., Caccia, S., and Campiani, G. (2001) *J. Biol. Chem. 276*, 44653−62.
14. Dixon, M., and Webb, E. C. (1979) *Enzymes*, 3rd ed., Longman, London.
15. Hays, H., and Berdis, A. J. (2002) *Biochemistry 41*, 4771−8.
16. Garcia-Diaz, M., Dominguez, O., Lopes-Fernandez, L. A., de Lera, L. T., Sangier, M. L., Ruiz, J. F., Parraga, M., Gacia-Ortiz, M. J., Kirchhoff, T., delMazo, J., Bernad, A., and Blanco, L. (2000) *J. Mol. Biol. 301*, 851−67.
17. Meyer, P. R., Matsuura, S. E., So, A. G., and Scott, W. A. (1998) *Proc. Natl. Acad. Sci. U.S.A. 95*, 13471−6.
18. Urban, S., Fischer, K. P., and Tyrrell, D. L. (2001) *Proc. Natl. Acad. Sci. U.S.A 98*, 4984−9.
19. Arion, D., Kaushik, N., McCormick, S., Borkow, G., and Parniak, M. A. (1998) *Biochemistry 37*, 15908−17.

20. Deibel, M. R., and Coleman, M. S. (1980) *J. Biol. Chem. 255*, 4206−12.
21. Pelletier, H., Sawaya, M. R., Kumar, A., Wilson, S. H., and Kraut, J. (1994) *Science 264*, 1891−903.
22. Pelletier, H., Sawaya, M. R., Wolfle, W., Wilson, S. H., and Kraut, J. (1996) *Biochemistry 35*, 12742−61.
23. Sawaya, M. R., Pelletier, H., Kumar, A., Wilson, S. H., and Kraut, J. (1994) *Science 264*, 1930−5.
24. Versieck, J., and Cornelis, R. (1989) *Trace Elements in Human Plasma or Serum*, CRC Press, Boca Raton, FL.

BI034198M